Ceramics International xxx (xxxx) xxx–xxx

Contents lists available at ScienceDirect

Ceramics International

journal homepage: www.elsevier.com/locate/ceramint

Microstructural, mechanical and biological properties of hydroxyapatite - $CaZrO_3$ biocomposites

Mariana F. Vassal[a], J. Nunes-Pereira[a], Sónia P. Miguel[b], Ilídio J. Correia[b], Abílio P. Silva[a,*]

[a] Centre for Mechanical and Aerospace Science and Technologies (C-MAST), Universidade da Beira Interior, Rua Marquês d'Ávila e Bolama, 6201-001 Covilhã, Portugal
[b] CICS-UBI-Centro de Investigação em Ciências da Saúde, Universidade da Beira Interior, Av. Infante D. Henrique, 6200-506 Covilhã, Portugal

ARTICLE INFO

Keywords:
Hydroxyapatite
Calcium zirconate
Ceramic biocomposites
Mechanical properties
Bioactivity

ABSTRACT

The biofunctionalization of metal implants with bioactive ceramics arises as an appealing strategy for promoting their osseointegration, without impairing implants' good mechanical resistance. In this work, biocomposites of hydroxyapatite - $CaZrO_3$ were obtained by rate controlled sintering and their microstructure, mechanical properties, biological as well as the effect of stoichiometric calcium zirconate dopant on the decomposition of HA were analysed. The results obtained showed that the addition of $CaZrO_3$ stabilizes the hydroxyapatite at least up to 1300 °C and inhibits the appearance of the α- and β-TCP phases. Moreover, the mechanical properties of the hydroxyapatite were improved with 10 wt% of $CaZrO_3$, despite the increase of porosity. The *in vitro* assays demonstrated that the biocomposites were biocompatible, since they favoured human osteoblast cells adhesion and proliferation. All the data obtained emphasize the potential of these biocomposites for the aimed biomedical application.

1. Introduction

The human life expectancy has been increasing, leading to the aging of world population. Older people usually suffer from health complications, namely related to bone tissue and joints (*e.g.* osteoarthritis and osteoporosis) [1]. These pathologies lead to the degeneration of the articular cartilage and to a decrease in bone mineral density (BMD), which makes the bone structure more porous and fragile, *i.e.* more susceptible to fractures and tumours in cartilage and bone tissue [2]. In addition, an increase in the sport injuries or other types of trauma caused, for example, by road accidents have been reported among the active population.

In order to patients regain the quality of life, it is mandatory to restore the structure and functions of the musculoskeletal system [2]. To accomplish that, in recent years there has been an increase in the number of artificial implant surgeries to treat musculoskeletal disorders (*e.g.* 4.9 million in 2002 to 39.7 million in 2010). In addition, the number of implant revision surgeries of hip and knee replacements is predicted to increase exponentially (137% and 601%, respectively) between 2005 and 2030 [3,4]. Longer lasting implants with optimized properties, may be a good therapeutic approach, since they will contribute to reduce the number of revision surgeries, as well as the patients' costs, discomfort and pain [5].

Orthopaedic implants with supporting function are mostly manufactured using biometals, such as stainless steel (316 L), titanium (Ti) alloys, nickel (Ni) and cobalt-chromium (CoCr) alloys [6]. These medical devices are widely used in the repair and replacement of a degraded or inhibited function of the locomotor system, such as knees, hips, shoulders, spine joints, dentistry and orthopaedic fasteners such as pins and bolts [3,7,8]. These materials exhibit high mechanical strength, good workability, resistant to corrosion (biotolerable) and low cost [8–10]. Although, they present some limitations, namely high density, stress shielding phenomenon, which induces re-fracture, and "only" biotolerance of these inert metallic devices [1,8]. Such inability to interact with living tissue (chemical inertia) will inhibit their biological fixation and osseointegration [11,12].

In addition, over the years there is an inevitable aseptic weakening and wear of the metal surface with the consequent release of nanoparticles and ions into the biological system, causing several clinical symptoms and impairment of organs function [13–15]. On the other hand, bioactive ceramic promotes the interaction with ions, biomolecules and cells, minimizing materials cytotoxicity, stimulating osseointegration and with the possibility of using different geometries and manufacturing techniques [16–24]. Among different available bioceramics, the hydroxyapatite (HA: $Ca_{10}(PO_4)_6(OH)_2$) based material have triggered a particular interest from researchers and clinicians since they have a chemical composition similar to the human bone, induce bone tissue growth and have a high thermodynamic stability

* Corresponding author.
E-mail address: abilio@ubi.pt (A.P. Silva).

https://doi.org/10.1016/j.ceramint.2019.01.122
Received 27 November 2018; Received in revised form 8 January 2019; Accepted 16 January 2019

under physiological conditions, such as temperature, pH and in contact with body fluids. Nevertheless, they present low mechanical strength and high brittleness, which restricts its application to areas where lower mechanical stress is required [25–30].

In this way, the ceramic composites of HA reinforced by particles or fibres of fully stabilized zirconia (YFSZ: ZrO_2-Y_2O_3, 92:8 mol.%) can combine the biocompatibility of HA with the high strength and fracture toughness of zirconia [30,31]. However, several studies described that the use of Y_2O_3 entails disadvantages particularly its degradation even at low temperatures, a phenomena known as "ageing phenomenon" [32,33]. In this case, water molecules react with Y_2O_3, forming clusters rich in $Y(OH)_3$, affecting the stability of tetragonal zirconia (t-ZrO_2) allowing its transformation into a monoclinic structure (m-ZrO_2) [34]. Other limitations are related with the decomposition of HA into tri-calcium phosphate (TCP) at ~1300 °C. Further, the diffusion of calcium from the HA into the zirconia phase leads to the formation of a cubic calcia-stabilized zirconia, and subsequently calcium zirconate ($CaZrO_3$) [32,35,36]. Calcium zirconate presents a high chemical stability (stoichiometric congruent reaction at ~2365 °C) [37] and an excellent corrosion resistance against alkali environments [38], as well as a thermal barrier coating (TBC) [39,40]. Furthermore, the calcium zirconate can be sintered in an oxide atmosphere (low cost), and the resultant material displays surface properties (wear), modulus of elasticity and hardness that are compatible with its application in structural support [41–43]. Moreover, calcium zirconate displays a high affinity with titanium and its alloys, making it a potential candidate for biomedical applications [44,45].

The aim of this work was to produce $CaZrO_3$-HA composites obtained by rate controlled sintering and then characterize their microstructure, porosity, effect of stoichiometric calcium zirconate dopant on the decomposition of HA, mechanical and biological properties.

2. Experimental

As starting materials hydroxyapatite, $Ca_{10}(PO_4)_6(OH)_2$ (HA, Alfa Aesar) and calcium zirconate, $CaZrO_3$ (CZ, Alfa Aesar) powders were used as ingredients to produce three different types of HA-CZ biocomposites (90HA10CZ and 80HA20CZ), concerning the amount of 10 and 20 wt% of CZ, respectively. In addition, 100 wt% hydroxyapatite samples (100HA) were fabricated for future reference as shown in Table 1.

In order to obtain fine grained and homogeneous ceramic biocomposites, the powders used in each mixture were milled during 2 h using isopropyl alcohol as a mixing media and zirconia balls of 3 mm diameter. The laser particle size analyser Coulter LS200 was used to control particle size distribution evolution of the mixture during the milling process.

The mixtures were dried at 60 °C for 24 h, sieved through a 63 μm mesh, uniaxially pressed at 25 MPa into discs (ϕ = 10 mm and t = 2 mm), and then sintered at 1300 °C for 2 h. Using Archimedes method (ASTM C20), the density (ρ) and apparent porosity (AP) of the sintered materials were measured. The relative density (TD) was determined by the Archimedes method, using the theoretical densities calculated from the X-ray diffraction (XRD) analysis. Strength of the materials sintered at 1300 °C was determined by the Diametral Compression of Discs Test (DCDT), conducted in Shimadzu AGS-X universal testing machine, with a speed of 0.5 mm/min. The tensile strength (σ_f) was determined by the Eq. (1) using a least of 10 valid specimens.

Table 1
Compositions and particle size of HA-CZ ceramic biocomposites.

Samples	HA (wt%)	$CaZrO_3$ (wt%)	d_{50} [μm]	SSA [cm^2/g]
100HA	100	0	1.61	14,129
90HA10CZ	90	10	1.40	14,128
80HA20CZ	80	20	1.19	15,014

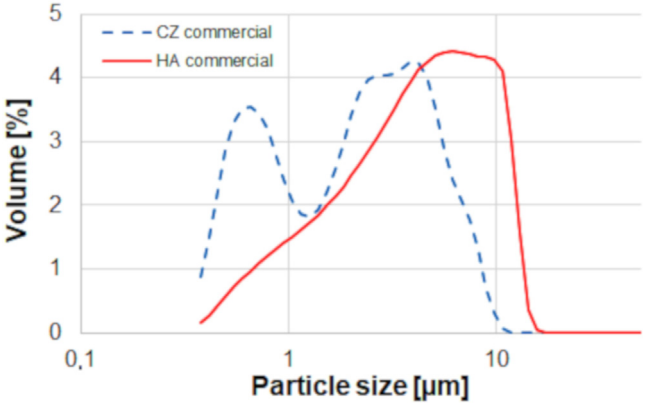

Fig. 1. Particle size distribution of commercial raw materials (Hydroxyapatite, HA and calcium zirconate, CZ).

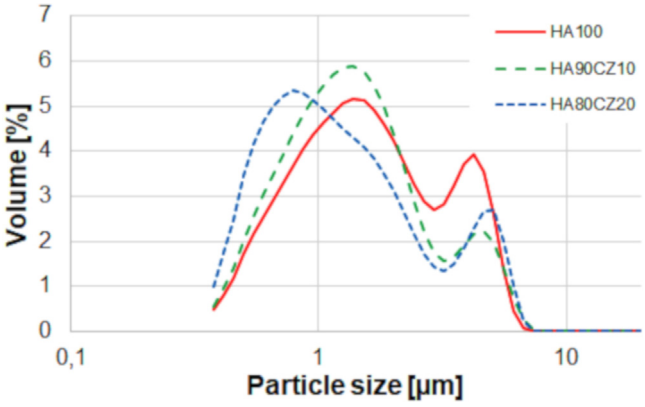

Fig. 2. Particle size distribution of the three HA-CZ ceramic composites after 2 h of milling.

Table 2
Properties of HA-CZ ceramic biocomposites sintered.

Samples	AP [%]	ρ [g/cm^3]	TD [%]	σ_f [MPa]	H [GPa]
100HA	0.52 ± 0.2	3.08 ± 0.1	98	18.9 ± 3.2	4.2 ± 0.1
90HA10CZ	1.61 ± 0.4	3.03 ± 0.1	87	37.5 ± 4.2	4.6 ± 0.1
80HA20CZ	16.07 ± 0.4	2.79 ± 0.1	74	24.4 ± 3.9	2.6 ± 0.1

$$\sigma_f = \frac{F}{A} = \frac{2F}{\pi D t} \quad (1)$$

where "F" is the diametral compression fracture force and "A", "D" and "t" are the discs' area, diameter and height, respectively.

Therefore, all fractured samples were analysed by scanning electron microscopy (SEM, Hitachi S3400N) to ensure that fracture was not originated by extensive local crushing close to the loading points. Representative half parts resulting from the DCDT, were embedded in EpoFix resin (Struers) and polished to assess microstructure features, after thermal etching using SEM analysis. Vickers hardness tests were also conducted in similar polished samples in Mitutoyo AVK-C2, according ASTM C1327. Dimensions of the residual imprints were used to determine the hardness H according the Eq. (2).

$$H_V = \frac{P}{A_T} = 1.8544\frac{P}{d^2} \quad (2)$$

where "P" is the applied force (50 N), A_T is the true contact area and "d" the diagonal dimensions average (mm).

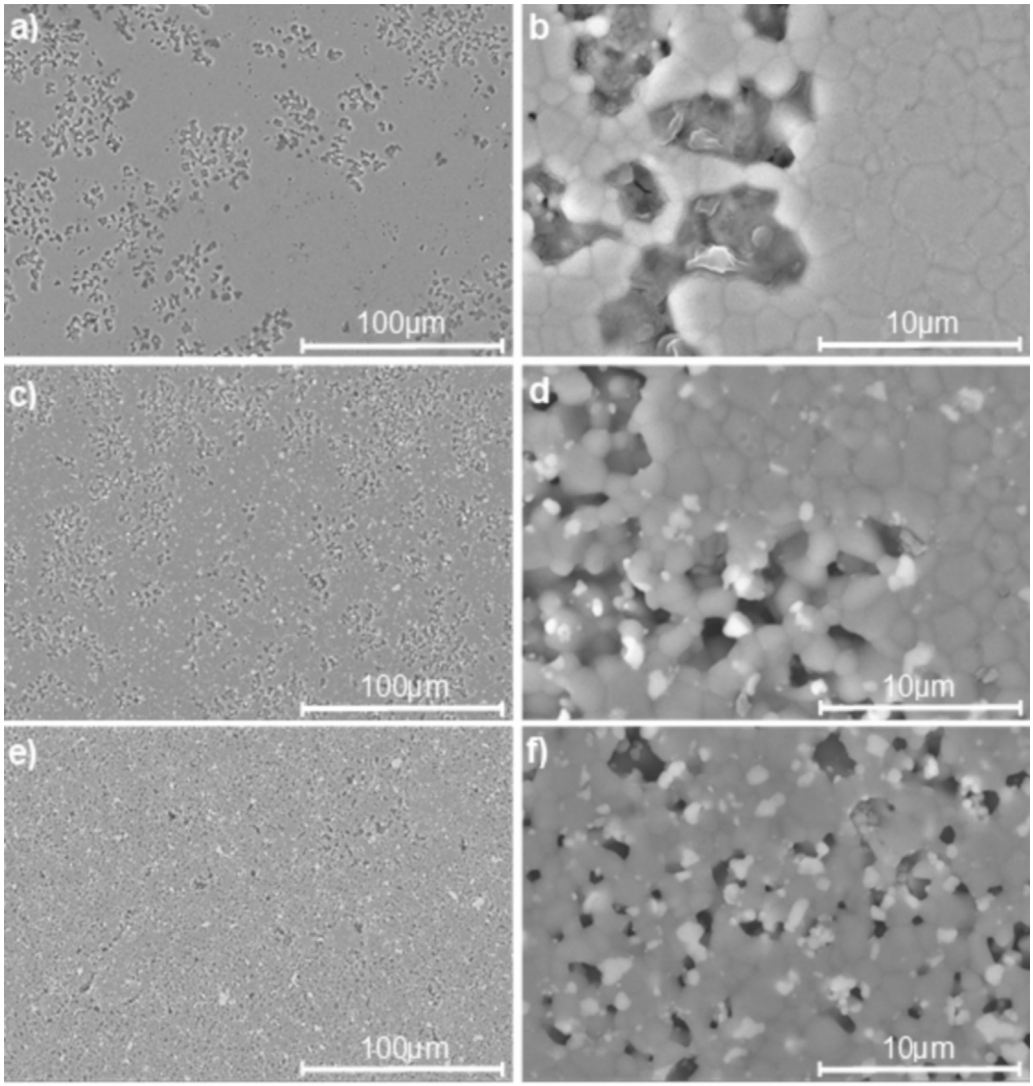

Fig. 3. Characteristic microstructural features of HA-CZ ceramic composites sintered at 1300 °C. SEM micrographs of polished surfaces: a) HA100, c) 90HA10CZ and e) 80HA20CZ low magnification (500×); b) HA100, d) 90HA10CZ and f) 80HA20CZ high magnification (5000×).

Lateral cracks were also measured in order to calculate the toughness [46], however the high porosity of the materials and the deformation due the densification below the mark during application of the force did not allow to obtain reliable data. The phase composition of the sintered biocomposites was determined by XRD measurements with CuKα radiation (Rigaku, model DMAX III/C). The main phase content was quantified using the Rietveld analysis.

The cytotoxic profile of HA-CZ biocomposites was evaluated *in vitro,* following ISO10993-5. Prior to cell seeding, the samples were placed into 48-well plates and sterilized by UV irradiation during 1 h. Human osteoblast (hOB) cells were used as model cells and seeded at a density of 2×10^4 cells per well. The plate was incubated at 37 °C, in a 5% CO_2 humified atmosphere. Then, the evaluation of cell morphology and proliferation in contact with the biomaterials was performed by the acquisition of microscopic images after 1, 3 and 7 days of incubation. Posteriorly, an MTT assay was performed at pre-determined timepoints. The metabolic conversion of MTT to purple formazan crystals occurs in living cells and such process allows to determine the metabolic activity of the viable cells present in each well. Briefly, the medium was removed and 100 µL of MTT (5 mg/mL PBS) were added to each sample (n = 5) followed by their incubation for 4 h in 5% CO_2 atmosphere. Furthermore, cells were treated with 400 µL of DMSO (0.04 N) for 30 min, dissolving the formazan crystals. A microplate reader (*Bio-rad xMark* microplate spectrophotometer) was used to quantify the absorbance at 570 nm of the samples from each well. Cells cultured without materials were used as a negative control (K^-), whereas cells cultured with EtOH (80%) were used as a positive control (K^+).

In addition, the cellular attachment to HA-CZ biocomposites surface was assessed by SEM analysis (Hitachi S-3400N). Samples containing cells were fixed for 30 min with 2.5% (v/v) glutaraldehyde. After, samples were washed and frozen at −80 °C and freeze-dried for 3 h. Then, samples were coated with gold through a Quorum Q150R ES sputter coater.

3. Results

The particle size distribution of the raw materials used in each mixture was analysed (Fig. 1), with CZ having a bimodal size distribution (0.69 and 4.05 µm, d_{50} = 2.30 µm) while HA has a semi-Gaussian distribution (d_{50} = 4.48 µm). In Fig. 2, the particle size distribution curve of the HA-CZ composites has shifted to the left after an increased milling time (2 h), corresponding to smaller particle sizes with an average size (d_{50}) of the same order and specific surface area (SSA) identical (Table 1).

The apparent porosity, as measured with the Archimedes technique in distilled water, presents an average value of 0.52%, 1.61% and

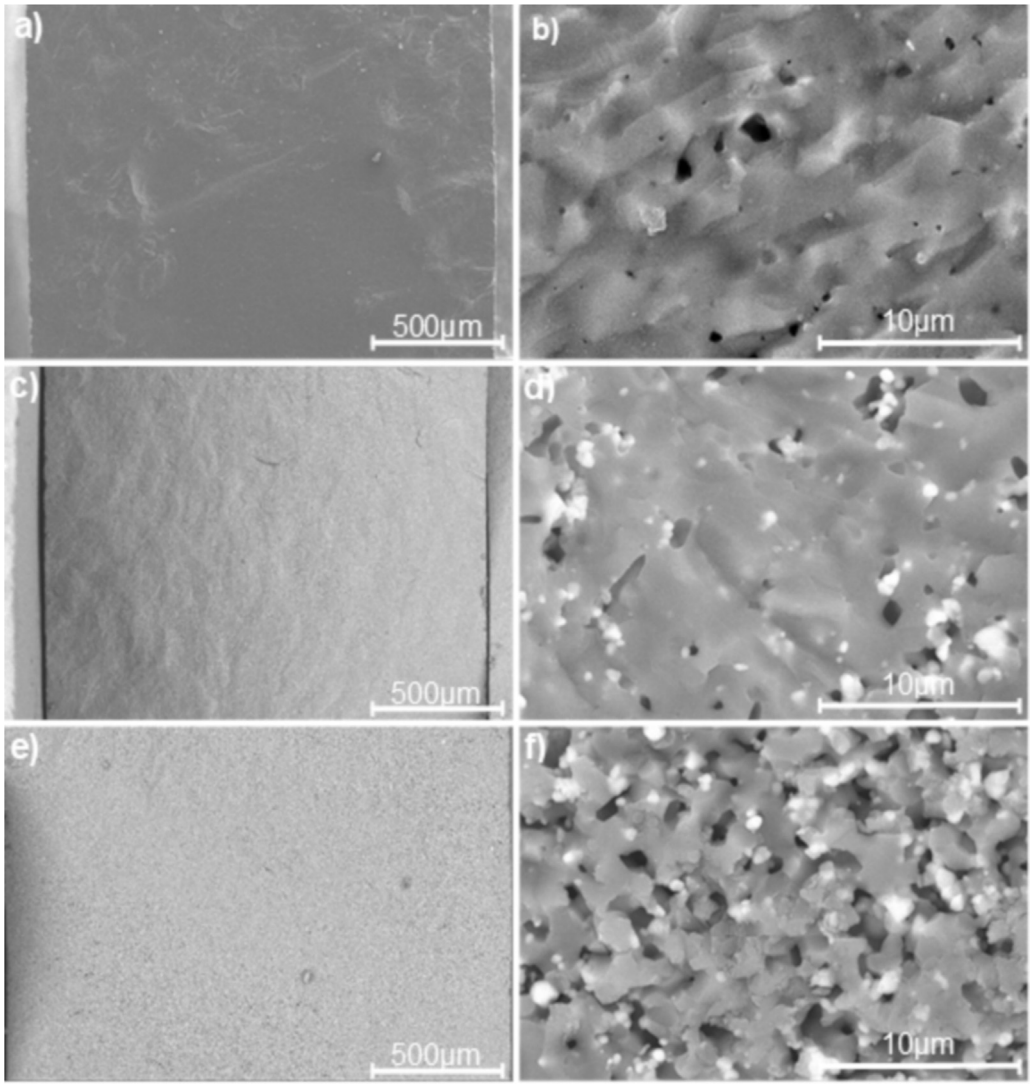

Fig. 4. Characteristic fracture surface of HA-CZ ceramic composites sintered at 1300 °C: a), c) and e) low magnification (65×); b), d) and f) high magnification (5000×).

16.07% for 100HA, 90HA10CZ and 80HA20CZ materials, that is followed by a density around 3.08 g/cm^3, 3.03 g/cm^3 and 2.79 g/cm^3, respectively (Table 2).

DCDT mechanical tests were then performed to assess the tensile strength of the sintered ceramic biocomposites. The results obtained showed that the composites which contain 10 wt% $CaZrO_3$ are significantly stronger than the other compositions, with a superior strength of 37.5 MPa (Table 2). As expected, with an additional increase in porosity (from TD of the 87–74%), as in the 80H20CZ samples, a lower resistance value of 24.4 MPa was obtained.

Vickers hardness tests showed a slightly higher hardness for the 90HA10CZ materials compared to 100HA, besides of the increase of porosity, with a value of 4.6 GPa and 4.2 GPa, respectively. These values decreased with $CaZrO_3$ content of 20 wt%, resulting in a hardness of 2.6 GPa, which is significantly inferior.

Microstructural features of three ceramic biocomposites sintered at 1300 °C are shown in Fig. 3. All specimens were constituted by continuous matrices with pores (5–10 µm), however the number and depth of the pores increased with the content of CZ. In turn, the microstructure of the composites shows inhomogeneity, consisting in hydroxyapatite (grey areas) and zirconia phases (light particles).

In Fig. 4, the characteristic fracture surfaces of the three sintered materials are displayed. It was not possible to discern any large defect as obvious fracture origin. At low magnification, fracture was much more tortuous in samples 90HA10CZ than in the other ones (Fig. 4a, c, and d).

XRD patterns of HA100, HA90CZ10 and HA80CZ20 biocomposites sintered at 1300 °C for 2 h are presented in Fig. 5. Due to the high temperature of sintering, the HA began to decompose to a mixture of α- and β-TCP. The specimens of HA90CZ10 and HA80CZ20 show the presence of calcium zirconate in their compositions. X-ray diffraction spectra of theoretical cards of the possible decomposed phases of HA (α- and β-TCP), $CaZrO_3$ (m-ZrO_2; t-ZrO_2; c-ZrO_2), and of the possible decomposed of the both initial phases (CaO) are also presented in order to facilitate the analysis.

The biocompatibility of the ceramic biocomposites was characterized using an MTT assay. Herein, the human osteoblasts (hOB) were used as model cells since these cells are responsible for the production and the remodelling of bone matrix [47], which is essential in the osseointegration process. Optical microscopic images were acquired of hOB cells cultured in contact with 100HA, 90HA10CZ and 80HA20Z samples at different timepoints. These images presented in Fig. 6, show that hOB cells proliferate and did not suffer any morphological variation when in contact with the bioceramics. Additionally, the cytotoxic profile of the biocomposites was further evaluated through an MTT assay during 1, 3 and 7 days. The results obtained (Fig. 7) showed that

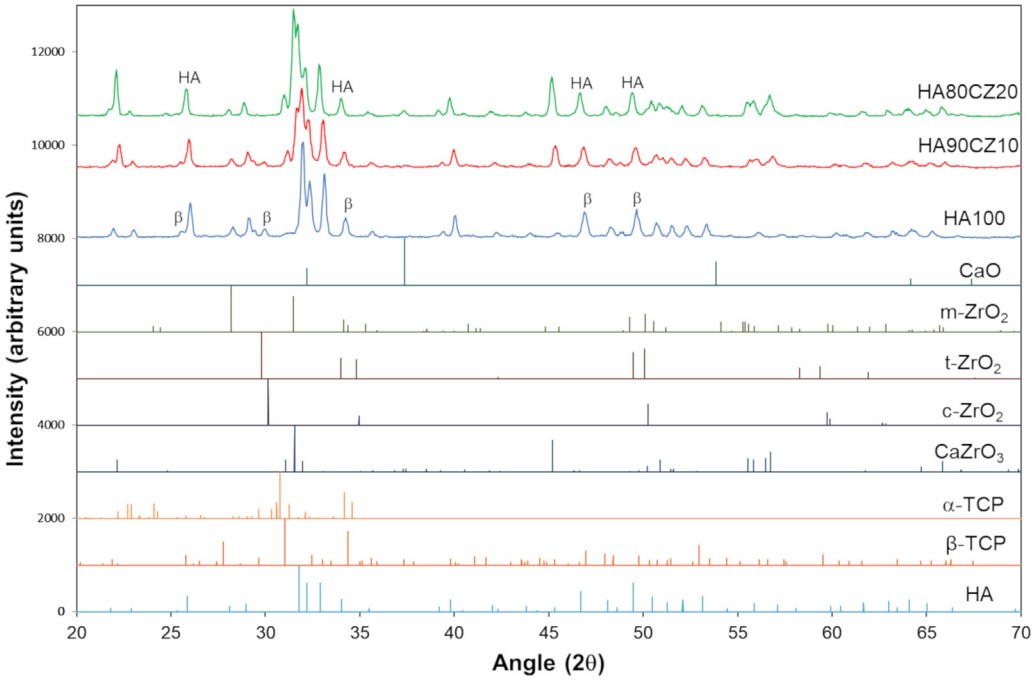

Fig. 5. X-ray diffraction spectra of the sintered composites and of the theoretical patterns of the possible phases. From top to bottom: HA80CZ20; HA90CZ10; HA100; CaO (#4–777); m-ZrO2 (#37–1484); t-ZrO2 (#17–923); c-ZrO2 (#49–1642); CaZrO3 (#35–0790); α-TCP (#9–348); β-TCP (#9–169); HA (#9–432).

hOB cell remained metabolically active in contact with the samples, even after 7 days of incubation. To further assess the applicability of the biocomposites for the intended biomedical application, hOB cell adhesion and cell morphology was characterized. As observed in Fig. 8, the cells adhere and proliferate onto the surface of the biocomposites after 1 day. Moreover, after 7 days, the spreading of cells occurs, revealing the excellent surface features of the biocomposites.

4. Discussion

In production of the materials for biomedical applications, it is required that the material can provide structural support for the formation of the new tissue as well as improve the healing process through the interaction with cells. To accomplish that, an ideal material must be porous to promote the cell adhesion and proliferation, but also must have sufficient mechanical strength to support the exerted forces during the regeneration process [47,48]. Therefore, biomaterial implants must combine the porosity with mechanical strength. Herein, this strategy was explored through the combination of HA with CZ.

After 2 h of milling, a tendency for a bimodal distribution of the HA-CZ ceramic composite decrease (Fig. 2), with an adjustment of the particle size of HA to the size of CZ powders, that is, the coarser particles begin to decrease in size, increasing the quantity of finer particles (Table 1): - d_{50} are 1.61 μm, 1.40 μm and 1.19 μm for HA100, HA90CZ10 and HA80CZ20, respectively. Also, the SSA (specific surface area) is similar for all samples (14,128–15,014 cm^2/g). This ensures that all materials are processed with similar finer and more homogenous powders.

From Table 2, it can be observed that with an addition of 20 wt% $CaZrO_3$, the porosity continuously increased until it reaches the maximum value of 16%, having the lowest density value (2.79 g/cm^3) of all three compositions. The relative density (TD) also decreases significantly with the addition of calcium zirconate. Such result was already reported by others authors [32,49], and can be and attributed to the effect of high temperature of sintering (1300 °C). The higher temperature leads to the agglomeration of the calcium zirconate particles, promoting lower sinterability and higher porosity.

In the diametrical compression test, the greatest tensile strength is uniform along the central part of the diametral plane of the disc, near of the compressive load supports in compression. The compression value is smaller for higher stiffness specimens because $t/D \leq 0.25$ ensures plane stress conditions. Failure occurs over the diametrical plane and the specimens are broken in two similar parts, which corresponds to a catastrophic drop in the load - displacement curve recorded during the test [50,51]. For the almost dense HA specimens (98%) it was obtained a tensile strength of 18.9 ± 3.2 MPa superior of the 4 MPa presented by Khoshsima et al. [52] in similar conditions. The hardness of 4.2 ± 0.1 GPa was in the same order of that reported by other works [31,32,36,52].

It can be noticed that yttria and calcia-stabilised zirconia addition lead to the increased strength and the hardness of the composites as compared to the "pure" hydroxyapatite samples [32]. In fact, the addition of 10% of $CaZrO_3$ increased the strength to 37.5 ± 4.2 MPa, the hardness to 4.6 ± 0.1 GPa as well as the porosity. Nevertheless, the 20% of $CaZrO_3$ presented the $\sigma = 24.4 \pm 3.9$ MPa and $H = 2.6 \pm 0.1$ GPa. The elastic and plastic properties of brittle ceramics are typically functions of the microstructure characteristic, such us grain size, porosity and the presence of secondary phases.

Assuming zero porosity through the equation proposed by Rice [53] is obtained for the composite 90HA10CZ: $\sigma_0 = 55.39$ MPa and H = 6.79 GPa, and for the composite 80HA20CZ: $\sigma_0 = 53.23$ MPa and H = 5.67 GPa. In this way, it is verified that by uniformizing the porosity effect, there is a considerable increase (2.8 times) of the mechanical resistance with the addition of 10% of calcium zirconate. However, an increase in the $CaZrO_3$ content did not promote an augment of the mechanical resistance.

The microstructures shown in Fig. 3 reveal that HA100 samples are composed of rounded grains with a mean size of 3 μm, but some of them are larger (~7 μm) and dense regions of β-TCP are visible due to decomposition of hydroxyapatite. Composites 90HA10CZ and 80HA20CZ present a similar typical grain size lower (2 μm) and more homogeneous with a maximum size up to 4 μm. In these composites no regions of β-TCP are observed, but pores with some depth and $CaZrO_3$ grains with size up to ~1 μm distributed along of the microstructure are observed.

In any of the fracture surfaces analysed (Fig. 4), there were no large

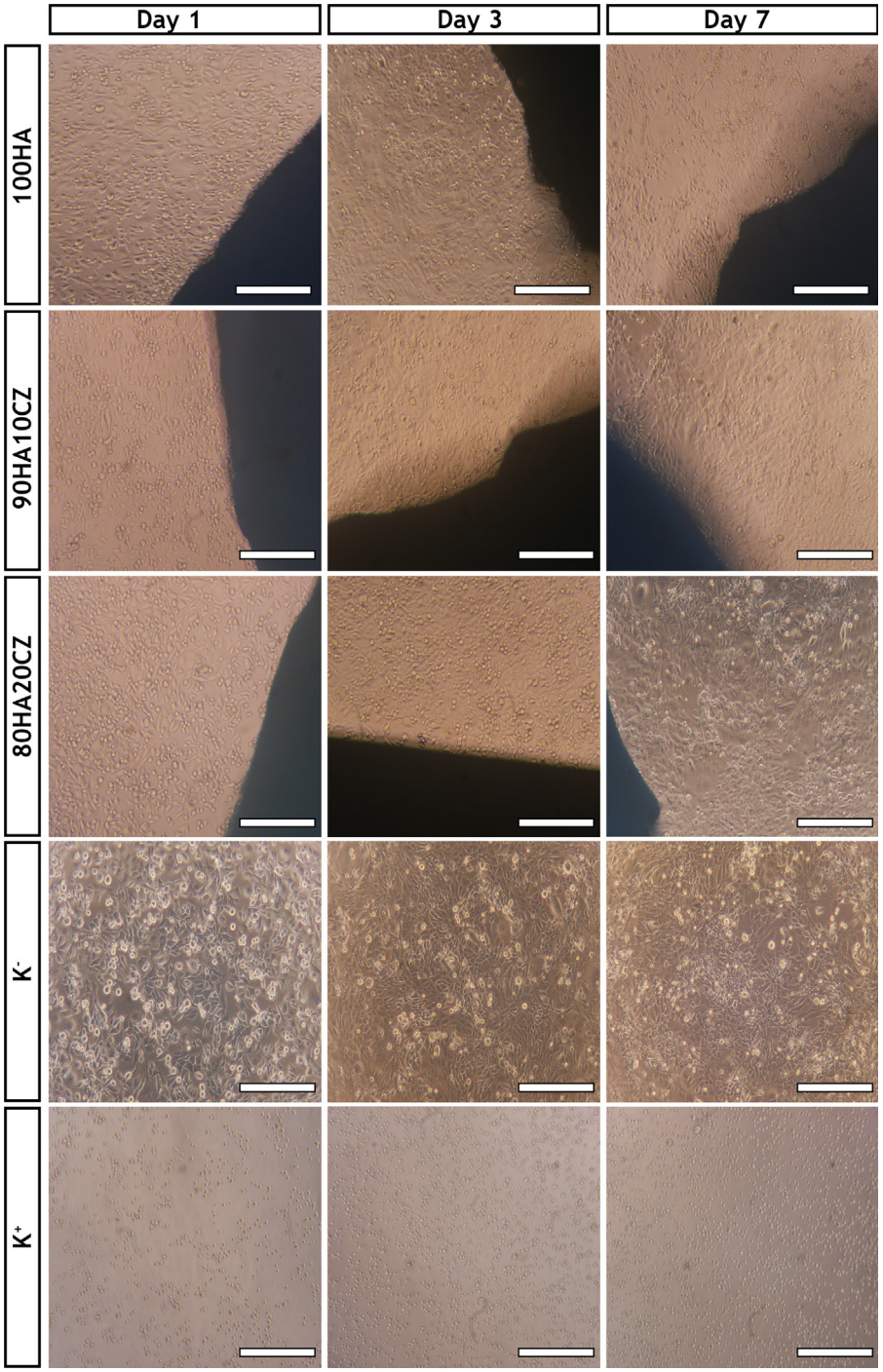

Fig. 6. Optical microscopic images of human osteoblasts (hOB) cultured on 100HA, 90HA10CZ and 80HA20CZ samples after 1, 3 and 7 days of incubation; K^-, negative control; K^+, positive control. Darker edges of the images correspond to the samples borders and shadows, where scale bar represents 200 μm.

singular defects. The main defects observed in the microstructure of the materials were pores, where the pore sizes were the smallest for material HA100, intermediate for material 90HA10CZ and largest for material 80HA20CZ. Therefore, large pores should act as critical flaws, and this would explain the lowest values of strength found for the 80HA20CZ material, despite the higher content of calcium zirconate. Fracture was mostly transgranular in HA100 specimens (Fig. 4a and b) and mixed transgranular/intergranular in 90HA10CZ (Fig. 4c and d) and 80HA20CZ (Fig. 4e and f). In H100 material, fracture was transgranular probably due to the large areas of glass areas. The finest and homogeneously distributed grains of $CaZrO_3$ and their strong grain boundaries surrounding by glass acting as effective cement between them can explain the greater relevance of the intergranular fracture. On the other hand, the high young modulus of $CaZrO_3$ (E = 228 GPa [41]) promotes the reinforcement of the hydroxyapatite matrix (E = ~95 GPa [32]) and consequently improve the resistance.

Samples composed of 100% hydroxyapatite (HA100) show peaks in 2θ of 25.80, 29.66, 34.37, 46.97 and 49.79 which are attributed to β-TCP (Fig. 5). Thus, it is confirmed that for pure hydroxyapatite samples there is a partial decomposition of β-TCP. Furthermore, in this analysis of the spectrum peaks, none of them can be attributed to the α-TCP phase, which is consistent with the literature [36,54], since the formation of this phase only occurs above 1350 °C.

In samples with 10% and 20% of calcium zirconate, the presence of

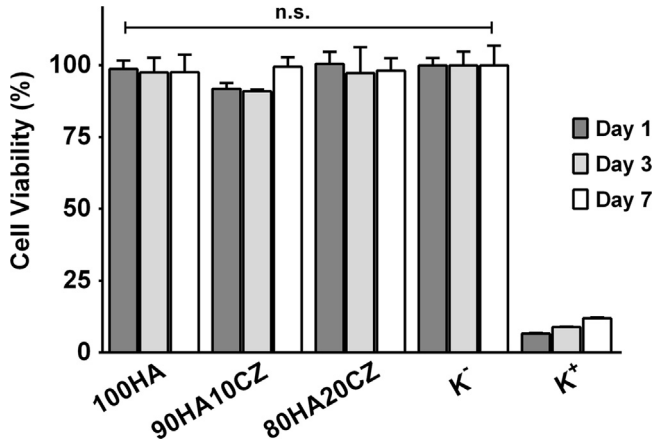

Fig. 7. Cellular viability after 1, 3 and 7 days compared to negative control (K^-), positive control (K^+) of the ceramic biocomposites with 0 wt%, 10 wt% and 20 wt% of $CaZrO_3$.

the peaks in 2θ of 22.07, 31.04, 31.54, 31.97, 45.18, 50.23, 50.89, 55.54, 55.86, 56.47 and 56.73 are observed (Fig. 5). These peaks are consistent with the theoretical $CaZrO_3$ phase card. The intensity of these peaks increase with higher contents of calcium zirconate. In these composites the formation of CaO and the order phases of zirconia (m-ZrO_2, t-ZrO_2 and c-ZrO_2) is not identified. The addition of the $CaZrO_3$ phase promoted the stabilization of the hydroxyapatite phase and did not lead to the formation of the β-TCP phase or the tetragonal phase (t-ZrO_2) [30,32]. This fact is based on the observation of the displacement of the peaks between the HA100 sample and the biocomposites (80HA20CZ): - displacement of the peak 25.80 (β-TCP) to 25.88 (HA); peak 34.37 (β-TCP) to 34.05 (HA); peak 46.97 (β-TCP) to 46.71 (HA); peak of 49.79 (β-TCP) to 49.47 (HA), and the absence of the peak 29.66 (β-TCP).

The major phases were determined by Rietveld refinement (Table 3), the sum of minority phases (CaO, m-ZrO_2, t-ZrO_2 and c-ZrO_2) is less than 1 wt%. The weight of the minority phases and the standard deviation explains why the indicated value for the CZ phase is greater than 20%. The results are consistent with Fig. 5, where the addition of $CaZrO_3$ promotes a gradual decrease of the HA decomposition in the α- and β-TCP phases.

In vitro studies were performed to determine bioactivity and biocompatibility of the biocomposites. The data obtained from MTT assay (Fig. 6) revealed that the different materials studied in this work with different content of HA and CZ did not affect viability of hOB cells, after 7 days of incubation. These results are in agreement with others, who previously investigated *in vitro* cytotoxicity of similar biocomposites with hydroxyapatite and ZrO2, and reported a reduced toxicity for these materials [55,56]. Such biocompatibility results can be explained by the presence of the hydroxyapatite in biocomposites. This bioactive mineral is also presented in mineral composition of native bone which is mainly composed by calcium and phosphate ions. Due to its similarity with the natural bone, HA can bind to a great variety of biomolecules and therefore, newly formed bone is able to directly attach to this material, thus making it an essential element required for bone regeneration [57–60].

The interaction between cells and samples surfaces was further analysed by SEM for 1, 3 and 7 days. The acquired images show that hOB cells were able to grow and spread on materials surfaces along time. These results can be attributed to surface roughness that has been reported to directly influence cellular morphology, proliferation and differentiation by providing a site for cellular adhesion and growth, rather than smooth surfaces [32,52,61,62]. Furthermore, among the tested compositions, 80HA20CZ samples seemed to present a lower number of adhered cells, a result that can be explained by its lower hydroxyapatite content.

Taking these results into consideration, it can be concluded that HA-CZ biocomposites are able to induce an appropriate cellular response, required for osseointegration between bone and implants, improves the mechanical strength without impairing biocompatibility. Nonetheless, for optimal balance between biological and mechanical results, HA-CZ

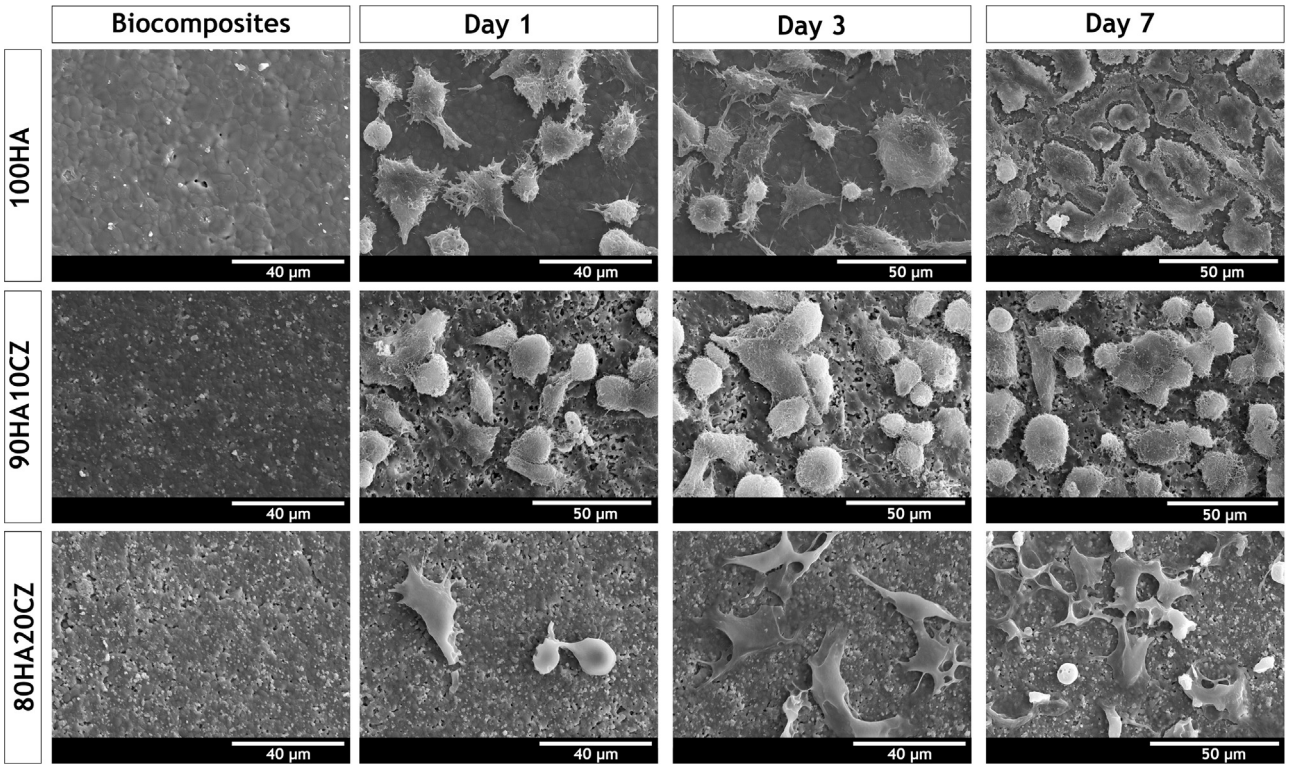

Fig. 8. SEM images of hOB cells at the surface of HA-CZ ceramic biocomposites after 1, 3 and 7 days.

Table 3
X-ray main phase composition of HA-CZ ceramic composites sintered obtained by Rietveld refinement.

Phases	100HA	90HA10CZ	80HA20CZ
HA	90.94 ± 0.1	84.55 ± 0.01	77.31 ± 0.01
β-TCP	9.07 ± 1.4	4.82 ± 0.68	1.21 ± 0.27
α-TCP	–	1.17 ± 0.63	–
CZ	0	9.46 ± 0.45	21.48 ± 1.03

biocomposites should be proposed as material for biomedical application, however for higher contents of 10 wt% $CaZrO_3$ the mechanical and biological properties start to decrease.

5. Conclusion

$CaZrO_3$-HA composites obtained by rate controlled sintering were manufactured and the effect of stoichiometric calcium zirconate dopant on the decomposition of hydroxyapatite, microstructural, mechanical and biological properties were studied.

The results obtained showed that the addition of 10 wt% of $CaZrO_3$ to the hydroxyapatite allowed the production of biocomposites with lower density values (1.6%), with a tensile strength and hardness for dense materials of the 55 MPa and 6.8 GPa, respectively. Moreover, the addition of the $CaZrO_3$ phase promoted the stabilization of the hydroxyapatite phase. The addition of higher values of $CaZrO_3$ increases the porosity and does not improve the mechanical and biological properties of the biocomposite.

Furthermore, the *in vitro* studies confirmed the good biocompatibility of the biocomposites, in particular for the composition with 10 wt% of $CaZrO_3$. These results high light the potential of this ceramic composition for biomedical applications being an alternative to the traditional applications of hydroxyapatite.

Acknowledgements

The authors are grateful for the support of the project Centro-01-0145-FEDER-000017 - EMaDeS - Energy, Materials and Sustainable Development, co-financed by the Portugal 2020 Program (PT 2020), within the Regional Operational Program of the Center (CENTRO 2020) and the European Union through the European Regional Development Fund (ERDF); and also the C-MAST - UID/EMS/00151 provided by FCT/MCTES through national funds (PIDDAC) and co-financed by the (European Regional Development Fund ERDF) through the Competitiveness and Internationalization Operational Program (POCI).

Sónia P. Miguel acknowledges individual PhD fellowship from FCT (SFRH/BD/109563/2015).

References

[1] V.P. Mantripragada, B. Lecka-Czernik, N.A. Ebraheim, A.C. Jayasuriya, An overview of recent advances in designing orthopedic and craniofacial implants, J. Biomed. Mater. Res. Part A 101 (2013) 3349–3364.
[2] U. Tarantino, M. Celi, C. Rao, M. Feola, I. Cerocchi, E. Gasbarra, A. Ferlosio, A. Orlandi, Hip osteoarthritis and osteoporosis: clinical and histomorphometric considerations, Int. J. Endocrinol. 2014 (2014) 372021.
[3] M. Geetha, A.K. Singh, R. Asokamani, A.K. Gogia, Ti based biomaterials, the ultimate choice for orthopaedic implants – A review, Prog. Mater. Sci. 54 (2009) 397–425.
[4] S. Kurtz, K. Ong, E. Lau, F. Mowat, M. Halpern, Projections of primary and revision hip and knee arthroplasty in the United States from 2005 to 2030, J. Bone Jt. Surg. Ser. A 89 (2007) 780–785.
[5] C. Lavernia, D.J. Lee, V.H. Hernandez, The increasing financial burden of knee revision surgery in the United States, Clin. Orthop. Relat. Res. 446 (2006) 221–226 (1976–2007).
[6] Q. Chen, G.A. Thouas, Metallic implant biomaterials, Mater. Sci. Eng. R Rep. 87 (2015) 1–57.
[7] Department of Research & Scientific Affairs, American Academy of Orthopaedic Surgeons. 〈www.aaos.org/research/stats/CommonProceduresTreatments-March2014.pdf〉. 2014.
[8] Buddy Ratner, Frederick J. Schoen, Jack E. Lemons, Biomaterials Science: An Introduction to Materials in Medicine, 2nd ed., Elsevier Academic Press, London, 2004.
[9] M. Saini, Y. Singh, P. Arora, V. Arora, K. Jain, Implant biomaterials: a comprehensive review, World J. Clin. Cases: WJCC 3 (2015) 52–57.
[10] F.F. Buechel, M.J. Pappas, Properties of materials used in orthopaedic implant systems, in: F.F. Buechel, M.J. Pappas (Eds.), Principles of Human Joint Replacement: Design and Clinical Application, Springer International Publishing, Cham, Switzerland, 2015, pp. 1–32.
[11] S. Parithimarkalaignan, T.V. Padmanabhan, Osseointegration: an update, J. Indian Prosthodont. Soc. 13 (2013) 2–6.
[12] M. Plecko, C. Sievert, D. Andermatt, R. Frigg, P. Kronen, K. Klein, S. Stübinger, K. Nuss, A. Bürki, S. Ferguson, U. Stoeckle, B. von Rechenberg, Osseointegration and biocompatibility of different metal implants - a comparative experimental investigation in sheep, BMC Musculoskelet. Disord. 13 (2012) (32-32).
[13] T. Hanawa, Overview of metals and biomedical applications, in: M. Niinomi (Ed.), Metal selection for biomedical devices, in Metals for Biomedical Devices, Woodhead Publishing, 2010, pp. 3–24 Part 1.
[14] G. Laing Patrick, B. Ferguson Albert, S. Hodge Edwin, Tissue reaction in rabbit muscle exposed to metallic implants, J. Biomed. Mater. Res. 1 (1967) 135–149.
[15] W.Z.W. Teo, P.C. Schalock, Metal hypersensitivity reactions to orthopedic implants, Dermatol. Ther. 7 (2017) 53–64.
[16] A. Vladescu, M.A. Surmeneva, C.M. Cotrut, R.A. Surmenev, I.V. Antoniac, Bioceramic coatings for metallic implants, in: I.V. Antoniac (Ed.), Handbook of Bioceramics and Biocomposites, Springer International Publishing, Cham, 2016, pp. 703–733.
[17] Y. Nayak, R.P. Rana, S.K. Pratihar, S. Bhattacharyya, Pressureless sintering of dense hydroxyapatite-zirconia composites, J. Mater. Sci. Mater. Med. 19 (2008) 2437–2444.
[18] X. Nie, A. Leyland, A. Matthews, Deposition of layered bioceramic hydroxyapatite/TiO_2 coatings on titanium alloys using a hybrid technique of micro-arc oxidation and electrophoresis, Surf. Coat. Technol. 125 (2000) 407–414.
[19] C.-L. Ko, Y.-Y. Chang, C.-H. Liou, W.-C. Chen, Characterization of the aspects of osteoprogenitor cell interactions with physical tetracalcium phosphate anchorage on titanium implant surfaces, Mater. Sci. Eng. C. 49 (2015) 7–13.
[20] A.P. Serro, C. Completo, R. Colaço, F. dos Santos, C.L. da Silva, J.M.S. Cabral, H. Araújo, E. Pires, B. Saramago, A comparative study of titanium nitrides, TiN, TiNbN and TiCN, as coatings for biomedical applications, Surf. Coat. Technol. 203 (2009) 3701–3707.
[21] R. Bosco, J. Van Den Beucken, S. Leeuwenburgh, J. Jansen, Surface engineering for bone implants: a trend from passive to active surfaces, Coatings 2 (2012).
[22] G. Soon, B. Pingguan-Murphy, K.W. Lai, S.A. Akbar, Review of zirconia-based bioceramic: surface modification and cellular response, Ceram. Int. 42 (2016) 12543–12555.
[23] H. Shao, J. He, T. Lin, Z. Zhang, Y. Zhang, S. Liu, 3D gel-printing of hydroxyapatite scaffold for bone tissue engineering, Ceram. Int. 45 (2019) 1163–1170.
[24] H. Shao, D. Zhao, T. Lin, J. He, J. Wu, 3D gel-printing of zirconia ceramic parts, Ceram. Int. 43 (2017) 13938–13942.
[25] N. Eliaz, N. Metoki, Calcium phosphate bioceramics: a review of their history, structure, properties, coating technologies and biomedical applications, Materials 10 (2017) 334.
[26] R.I.M. Asri, W.S.W. Harun, M.A. Hassan, S.A.C. Ghani, Z. Buyong, A review of hydroxyapatite-based coating techniques: sol–gel and electrochemical depositions on biocompatible metals, J. Mech. Behav. Biomed. Mater. 57 (2016) 95–108.
[27] E. Mohseni, E. Zalnezhad, A.R. Bushroa, Comparative investigation on the adhesion of hydroxyapatite coating on Ti–6Al–4V implant: a review paper, Int. J. Adhes. Adhes. 48 (2014) 238–257.
[28] M.M. Sebdani, M.H. Fathi, Preparation and characterization of hydroxyapatite–forsterite–bioactive glass nanocomposite coatings for biomedical applications, Ceram. Int. 38 (2012) 1325–1330.
[29] S. Ramesh, C.Y. Tan, R. Tolouei, M. Amiriyan, J. Purbolaksono, I. Sopyan, W.D. Teng, Sintering behavior of hydroxyapatite prepared from different routes, Mater. Des. 34 (2012) 148–154.
[30] M. Catauro, F. Bollino, E. Tranquillo, R. Tuffi, A. Dell'Era, S.V. Ciprioti, Morphological and thermal characterization of zirconia/hydroxyapatite composites prepared via sol-gel for biomedical applications, Ceram. Int. 45 (2019) 2835–2845.
[31] G. Ayoub, D. Veljovic, M.L. Zebic, V. Miletic, E. Palcevskis, R. Petrovic, D. Janackovic, Composite nanostructured hydroxyapatite/yttrium stabilized zirconia dental inserts – The processing and application as dentin substitutes, Ceram. Int. 44 (2018) 18200–18208.
[32] K. Castkova, H. Hadraba, A. Matousek, P. Roupcova, Z. Chlup, L. Novotna, J. Cihlar, Synthesis of Ca, Y-zirconia/hydroxyapatite nanoparticles and composites, J. Eur. Ceram. Soc. 36 (2016) 2903–2912.
[33] J. Chevalier, B. Cales, J.M. Drouin, Low-temperature aging of Y-TZP ceramics, J. Am. Ceram. Soc. 82 (1999) 2150–2154.
[34] F. Lange F, L. Dunlop G, I. Davis B, Degradation during aging of transformation-toughened ZrO_2-Y_2O_3 materials at 250 °C, J. Am. Ceram. Soc. 69 (1986) 237–240.
[35] X.F. Xiao, R.F. Liu, Y.Z. Zheng, Hydrothermal-electrochemical codeposited hydoxyapatite/yttria-stabilized zirconia composite coating, J. Mater. Sci. 41 (2006) 3417–3424.
[36] Z. Evis, M. Usta, I. Kutbay, Improvement in sinterability and phase stability of hydroxyapatite and partially stabilized zirconia composites, J. Eur. Ceram. Soc. 29 (2009) 621–628.
[37] S. Serena, A. Sainz Maria, A. Caballero, Experimental determination and thermodynamic calculation of the zirconia–calcia–magnesia system at 1600, 1700, and 1750 °C, J. Am. Ceram. Soc. 87 (2005) 2268–2274.

[38] S. Serena, M.A. Sainz, A. Caballero, The system Clinker–MgO–$CaZrO_3$ and its application to the corrosion behavior of $CaZrO_3$/MgO refractory matrix by clinker, J. Eur. Ceram. Soc. 29 (2009) 2199–2209.
[39] M. Khalid, M. Mujahid, A.N. Khan, R.S. Rawat, K. Mehmood, Effect of arc current on microstructure, texturing and wear behavior of plasma sprayed $CaZrO_3$ coatings, Ceram. Int. 39 (2013) 2293–2302.
[40] T. Karthikeya Sharma, Performance and emission characteristics of the thermal barrier coated SI engine by adding argon inert gas to intake mixture, J. Adv. Res. 6 (2015) 819–826.
[41] A.P. Silva, F. Booth, L. Garrido, E. Aglietti, P. Pena, C. Baudín, Young's modulus and hardness of multiphase $CaZrO_3$-MgO ceramics by micro and nanoindentation, J. Eur. Ceram. Soc. 38 (2018) 2194–2201.
[42] A. Silva, F. Booth, L. Garrido, E. Aglietti, P. Pena, C. Baudín, Sliding wear of $CaZrO_3$-MgO composites against ZrO_2 and steel, J. Eur. Ceram. Soc. 37 (2017) 297–303.
[43] F. Booth, L. Garrido, E. Aglietti, A. Silva, P. Pena, C. Baudín, $CaZrO_3$–MgO structural ceramics obtained by reaction sintering of dolomite-zirconia mixtures, J. Eur. Ceram. Soc. 36 (2016) 2611–2626.
[44] S. Schafföner, T. Qin, J. Fruhstorfer, C. Jahn, G. Schmidt, H. Jansen, C.G. Aneziris, Refractory castables for titanium metallurgy based on calcium zirconate, Mater. Des. 148 (2018) 78–86.
[45] M.D. Mathews, E.B. Mirza, A.C. Momin, High-temperature X-ray diffractometric studies of $CaZrO_3$, $SrZrO_3$ and $BaZrO_3$, J. Mater. Sci. Lett. 10 (1991) 305–306.
[46] G.R. Anstis, P. Chantikul, B.R. Lawn, D.B. Marshall, A critical evaluation of indentation techniques for measuring fracture toughness: i, direct crack measurements, J. Am. Ceram. Soc. 64 (1981) 533–538.
[47] T. Albrektsson, C. Johansson, Osteoinduction, osteoconduction and osseointegration, Eur. Spine J. 10 (Suppl 2) (2001) S96–S101.
[48] J. Caetano-Lopes, H. Canhão, J. Fonseca, Osteoblasts and Bone Formation, 2007.
[49] J. Brzezińska-Miecznik, K. Haberko, M. Sitarz, M.M. Bućko, B. Macherzyńska, R. Lach, Natural and synthetic hydroxyapatite/zirconia composites: a comparative study, Ceram. Int. 42 (2016) 11126–11135.
[50] I.H. García-Páez, R.G. Carrodeguas, A.H. De Aza, C. Baudín, P. Pena, Effect of Mg and Si co-substitution on microstructure and strength of tricalcium phosphate ceramics, J. Mech. Behav. Biomed. Mater. 30 (2014) 1–15.
[51] P. Jonsén, H.Å. Häggblad, K. Sommer, Tensile strength and fracture energy of pressed metal powder by diametral compression test, Powder Technol. 176 (2007) 148–155.
[52] S. Khoshsima, B. Yilmaz, A. Tezcaner, Z. Evis, Structural, mechanical and biological properties of hydroxyapatite-zirconia-lanthanum oxide composites, Ceram. Int. 42 (2016) 15773–15779.
[53] R. Rice, Porosity of Ceramics, CRC Press, Boca Raton, 1998.
[54] R. Ramachandra Rao, T.S. Kannan, Synthesis and sintering of hydroxyapatite–zirconia composites, Mater. Sci. Eng. C. 20 (2002) 187–193.
[55] R. Quan, D. Yang, X. Wu, H. Wang, X. Miao, W. Li, In vitro and in vivo biocompatibility of graded hydroxyapatite–zirconia composite bioceramic, J. Mater. Sci. Mater. Med. 19 (2008) 183–187.
[56] X. Ren, Q. Tuo, K. Tian, G. Huang, J. Li, T. Xu, X. Lv, J. Wu, Z. Chen, J. Weng, Q. Wang, Y. Mu, Enhancement of osteogenesis using a novel porous hydroxyapatite scaffold in vivo and vitro, Ceram. Int. 44 (2018) 21656–21665.
[57] M. Rouahi, O. Gallet, E. Champion, J. Dentzer, P. Hardouin, K. Anselme, Influence of hydroxyapatite microstructure on human bone cell response, J. Biomed. Mater. Res. Part A 78A (2006) 222–235.
[58] C. Wang, J. Ma, W. Cheng, R. Zhang, Thick hydroxyapatite coatings by electrophoretic deposition, Mater. Lett. 57 (2002) 99–105.
[59] K. Yamada, K. Imamura, H. Itoh, H. Iwata, S. Maruno, Bone bonding behavior of the hydroxyapatite containing glass–titanium composite prepared by the Cullet method, Biomaterials 22 (2001) 2207–2214.
[60] L.L. Hench, Bioceramics, J. Am. Ceram. Soc. 81 (2005) 1705–1728.
[61] D. Deligianni, N.D. Katsala, P. Koutsoukos, Y.F. Missirlis, Effect of surface roughness of hydroxyapatite on human bone marrow cell adhesion, Biomaterials (2001).
[62] H.I. Chang, Y. Wang, Cell responses to surface and architecture of tissue engineering scaffolds, regenerative medicine and tissue engineering, Cells and Biomaterials, 2011.